Journal of Applied Polymer Science

Effect of silane coupling agent on the fatigue crack propagation of silica-filled natural rubber

Hong Yao,[1,2] Gengsheng Weng, Yanpeng Liu, Kun Fu, Aijun Chang, Zhong-Ren Chen

[1]Department of Polymer Science and Engineering, Faculty of Materials Science and Chemical Engineering, Ningbo University, Ningbo 315211, People's Republic of China

[2]Ningbo Key Laboratory of Specialty Polymers, Ningbo 315211, People's Republic of China

Correspondence to: G. Weng (E-mail: wenggengsheng@nbu.edu.cn)

ABSTRACT: Based on the real-time crack tip morphology monitoring, the influence of silane coupling agent (SCA) on the crack-growth behavior of silica-filled natural rubber (NR) was analyzed. By using SCA, silica particles can be well dispersed and a filler–matrix network can be formed, which leads to lower crack-growth rate. Results indicate that a dosage of 5 wt % (with respect to silica loading) is the optimal content. The real-time observation and scanning electron microscopy (SEM) analysis proved that thin ligaments and dimples with homogeneous distribution appear on the crack tip. These crack tip morphologies reflect the low crack-growth rate. © 2015 Wiley Periodicals, Inc. J. Appl. Polym. Sci. **2015**, *132*, 41980.

KEYWORDS: elastomers; mechanical properties; rubber

Received 22 September 2014; accepted 10 January 2015
DOI: 10.1002/app.41980

INTRODUCTION

Because of the increasing fuel consumption and CO_2-emission, the concept of "Green tire" was proposed.[1] For its fine mechanical properties, age resistance, and low heat build-up,[2–5] silica has been established as a valuable choice for high performance passenger car tires manufacture.[6] By using silane coupling agent (SCA), it is possible to promote the dispersion of fillers in the rubber matrix and improve the filler–rubber interaction.[1] Many studies focused on the influence of SCA content on the change of dynamic mechanical behaviors, i.e., Payne effect, Mullins effect, and network structure.[7–12]

However, little attention has been paid to investigate the influence of SCA content on the crack-growth behavior. The property of fatigue fracture in rubber is fundamental for many rubber products. The failure of rubber products, which originates from crack growth, often results in catastrophic events.[13] To ensure the safety and reliability of rubber products, the research on crack propagation of rubber has a vital significance. Since tearing energy (T) as an analysis criterion of rubber crack-growth was proposed by Rivlin in 1953, crack-growth approach has been widely applied.[14–17] Nevertheless, most of the published studies that focus on crack growth tend to explain the fracture surface, and most of them are based on the pure mechanical theories.[18–20] The process of crack growth is often ignored.

In this article, the influence of SCA content on the crack-growth behavior was investigated. The crack-growth mechanism was also proposed according to the real-time crack tip morphology evolution. Based on the real-time crack tip morphology monitoring, we proposed some new insight into the crack-growth mechanism of natural rubber (NR) filled with silica.

EXPERIMENTAL

Materials and Specimens

NR was standard Vietnamese rubber (SVR3L). High dispersion silica 115GR with specific surface area of 160 m^2/g and pH of 6.45 were supplied by Rhodia (Qingdao, China). SCA bis-(triethoxysilylpropyl)-tetrasulfide (Si69), was purchased from Alfa Aesar (Tianjin, China).

Table Isummarizes the recipes of these composites and the percent in parentheses are weight of Si69 relative to silica content. Silica and Si69 were mixed in rubber on a two-roll mill at room temperature. Afterwards, the compounds were transferred to torque rheometer (HAPRO RM-200A) to ensure the reaction of the silane and silica surface. The temperature was held at 150°C for 10 min at a rotor speed of 35 rpm. The vulcanizates were cured at 150°C for 7 min.

Fatigue Loading Test and Real-Time Photographing

The fatigue tests were performed with the edge-notched specimens on a DMA setup (Metravib DMA+1000) with

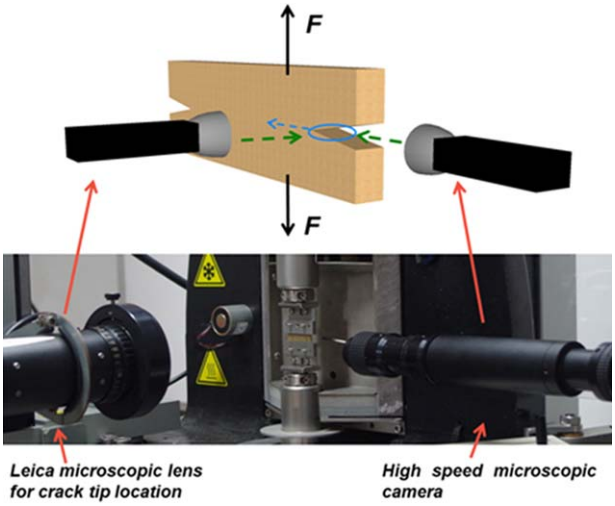

Figure 1. Experimental devices and working diagram. Blue ring represent the crack tip, blue arrow is crack direction. [Color figure can be viewed in the online issue, which is available at wileyonlinelibrary.com.]

crack-growth function. The specimens had the following dimensions: 35 mm in length, 8 mm in width, 2 mm in thickness. The initial crack was precut 1 mm in length at the edge of rubber by a sharp razor blade.

Crack-growth rates were measured under seven levels of T (J/m^2). The T values were given by the machine computation under the following three steps:

1. Applying a number of excitation cycles to the specimen to stabilize it.
2. Calculating the relation automatically between the energy delivered per area unit and loading displacement value and drawing the T curve which allows the displacement value to be applied for each cracking T value.
3. Choosing the corresponding displacement when the experimental condition is validated.

These tests were carried out at 23°C with a frequency of 10 Hz. The specimen was fixed in a fatigue loading apparatus (see Figure 1). The Leica microscope lens in the front was used to record the crack tip displacement (blue arrow) for calculating the rate. The ultra-high speed camera (Olympus i-speed 3) was placed on the side. It was employed to photograph the damage zone of crack tip in real-time.

Dynamic Mechanical Analysis

The viscoelastic properties of the specimens were measured under a dynamic tension mode at a frequency of 10 Hz on a conventional DMA (Metravib). The specimens were vulcanized to the following dimensions: 25 mm in length, 10 mm in width, 2 mm in thickness. The temperature range was from −80°C to 80°C at a heating rate of 5°C/min. The Payne effect tests were carried out at room temperature at 10 Hz in the dynamic strain range of 0–25%.

Determination of Crosslinking Density

The crosslinking density was determined by equilibrium swelling. Specimens were swollen in toluene at room temperature for 72 h and then removed from the solvent, and the toluene on the specimen surface was quickly blotted off with tissue paper. The specimens were immediately weighed on an analytical balance to the tolerance of 1 mg, and then vacuum dried. The crosslinking density was determined on the basis of the Flory–Rhener[21]:

$$-[\ln\ (1-\Phi_r)\ +\ \Phi_r+\ \chi\Phi_r{}^2]\ =V_0M_c\left[\Phi_r{}^{1/3}-\Phi_r/2\right] \qquad (1)$$

where Φ_r is the volume fraction of polymer in the swollen mass, V_0 is the molar volume of the solvent (106.2 cm^3 for toluene), M_c is cross-linking density, χ is the Flory–Huggins polymer–solvent interaction term. The value of χ for toluene—NR is 0.39. The value of Φ_r was reached according to the method used by Bala *et al*:[22]

$$\Phi_r=\frac{w2/\rho2}{\frac{w2}{\rho2}+(w1-w2)/\rho1} \qquad (2)$$

where w_1 and w_2 are the weights of the swollen and deswollen specimens, respectively, and ρ_1 and ρ_2 are the densities of the toluene and the cured rubber.

Scanning Electron Microscopy

The micro-morphologies of the specimens were performed with SEM (Su-70, Hitachi, Japan). Specimens were preprocessed under 2.0 × 10^4 cycles at a frequency of 10 Hz on the DMA+1000. Then, they were fractured in cryogenic temperature.

FTIR Analysis

FTIR analysis was carried out on a Nicolet 6700 FTIR spectrometer. The spectral range is 4000–400 cm^{-1}. A resolution of 4 cm^{-1} was chosen. It is noted that the unvulcanized samples were extracted by toluene for 48 h to remove the ungrafted Si69 and then dried in vacuum at 40°C for 12 h. These samples were pressed into pellets with KBr. The vulcanized samples were vulcanized into thin film for FTIR transmission analysis.

RESULTS AND DISCUSSION

Structure Characterization by FTIR

The grafting reaction occurs between the hydroxyl groups from silica and the silanol groups formed by hydrolysis of the SCA. Therefore, the grafting reaction between Si69 and silica can be identified by the appearance of characteristic bands in FTIR spectra, such as characteristic band of $\tilde{\nu}_{CH2}$ appearing at 2990–2920 cm^{-1}. Figure 2 shows FTIR spectra of silica, silica grafted Si69 (Si69-*g*-Silica) and Si69. It can be seen that the $\tilde{\nu}_{CH2}$ band exists in Si69-*g*-Silica, which is the evidence that Si69 molecules are grafted on the silica surface.

Ansarifar proved that the polysulfidic groups can react in the presence of accelerators at elevated temperatures (140–160°C) with or without sulphur being present, to form crosslinks in rubbers containing chemically active double bonds.[23] Although the characteristic absorption peak of NR appearing at 2990–2850 cm^{-1} in Figure 3 is overlapped with the $\tilde{\nu}_{CH2}$ band, which belongs to Si69-*g*-Silica, the $\tilde{\nu}_{as\ Si-O-Si}$ band at 1096 cm^{-1} and δ_{Si-OH} band at 958 cm^{-1} still can be seen on the IR spectrum of Si69-*g*-Silica-filled vulcanized NR. Hence, the chemical bonding between Si69 grafted filler and NR molecules is confirmed.

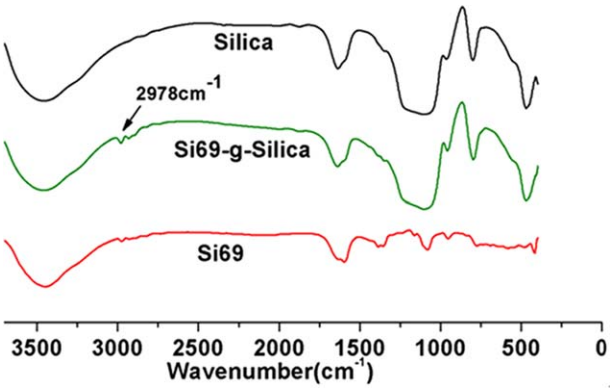

Figure 2. FTIR spectra of silica, Si69-*g*-Silica and Si69. [Color figure can be viewed in the online issue, which is available at wileyonlinelibrary.com.]

Crack-Growth Rate

Lake and Lindley[24,25] have proved that the crack-growth rate can be divided into four stages based on various tearing energies. In stage 1, T is lower than the threshold (T_0), the propagation length per cycle, dc/dn, is usually regarded as 0. In stage 4, dc/dn becomes very large when the T is higher than the critical value (T_c). Between the above two T values, which is stage 2, dc/dn proceeds linearly with increasing T:

$$dc/dn = A(T - T_0),\ T_0 < T < T_a \quad (3)$$

and stage 3,a power law:

$$dc/dn = \mathrm{BT}^b,\ T_a < T < T_c, \quad (4)$$

where c is the cracking length, n is the number of loading cycles, T_0, T_c, T_a, A, B are material constants, T_a is a transition value. The values of T_0 and T_c cannot be obtained because of the testing limitation of device, b should be determined experimentally.[24,26,27]

Figure 4 shows the crack-growth rates of silica-filled NR with different Si69 contents in each tearing energy on a logarithmic scale, which are in good agreement with the power law in eq. (4). The crack-growth rate decreases with increasing Si69 content. The dc/dn value reaches a minimum at about 5 wt % Si69 and shows an increasing trend thereafter. Table II lists the measured crack-growth parameters. The value of b is determined by the slope of the linear fitting. The lowest B and highest b indicate Si69 at low T values is more efficient to decrease the crack-growth rate.[28]

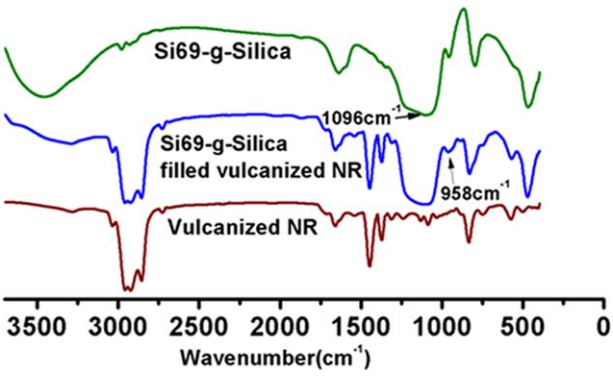

Figure 3. FTIR spectra of vulcanized samples compared with Si69-*g*-Silica. [Color figure can be viewed in the online issue, which is available at wileyonlinelibrary.com.]

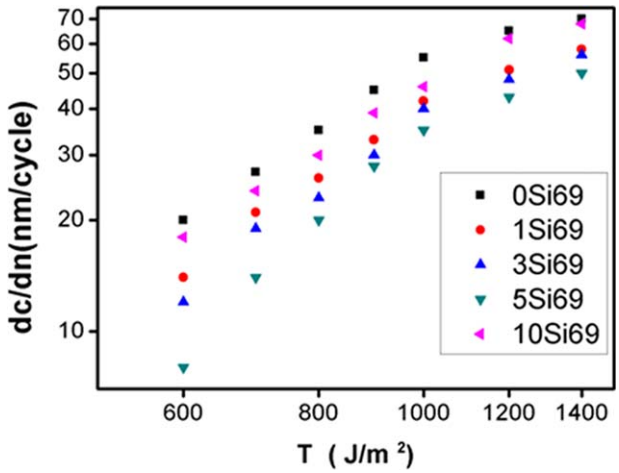

Figure 4. Crack-growth rates of specimens with different Si69 contents as a function of T. The inset represents the percent by weight of Si69 relative to silica content. [Color figure can be viewed in the online issue, which is available at wileyonlinelibrary.com.]

Viscoelastic Behavior

To explore the effect of the Si69 further, the nonlinear viscoelastic behavior was investigated. Figure 5 presents the Payne effect plots. The silica-filled NR without Si69 has a larger magnitude. When the Si69 is applied, the magnitude of the modulus at strain smaller than 8% decreases till Si69 content reaches 5 wt %. Thereafter, it increases again. The curve of 10 wt % Si69 is even higher than the 0 wt % Si69 at slightly higher strain amplitude (≥3%). It is well known that silica as a filler itself shows a very strong filler networking due to poor compatibility to hydrocarbon rubber, polar character and the ability of hydrogen bonding.[29] In this case, the filler networking leads to the increase of modulus.[29] As a bifunctional silane, the Si69 reduces filler-filler agglomeration. It implies that the filler networking can be reduced. Thus, the modulus at small strains decreases. Similar results were also reported in previous literatures.[29,31] When the Si69 content increases further, the plateau modulus

Table I. Recipes of Filled NR with Different Si69 Content

Material	Content (phr)
Natural Rubber (NR)	100
Zinc oxide	5
Stearic acid	2
Accelerator CZ[a]	1
Accelerator D[b]	2
Sulfur	2
Silica	30
Si69	0 (0%), 0.3 (1%), 0.9 (3%), 1.5 (5%), 3 (10%)

[a] N-Cyclo-hexyl-2-benzothiazolesulfenamide.
[b] 1,3-Diphenyl guanidine.

Table II. Fatigue Parameters of the Rubber Composites with Different Si69 Content

Composite	*B*	*b*
0Si69	−2.92	1.53
1Si69	−3.47	1.68
3Si69	−3.90	1.81
5Si69	−4.94	2.13
10Si69	−3.74	1.81

Table III. Crosslinking Density of Silica Filled NR with Different Si69 Contents

Composite	Crosslinking density (mol/mm^3)
0Si69	76.16
1Si69	75.49
3Si69	75.69
5Si69	76.58
10Si69	96.24

increases. This is because more and more chemical bondings[29,30] between the silica surface and the rubber matrix appear at the Si69 content of 10 wt %. It implies that the increasing of crosslinking dominates at high Si69 content (the crosslinking density results can be seen in Table III). So, the modulus is enhanced.

Figure 6 shows the loss modulus curves in the range of −80°C to 80°C at a frequency of 10 Hz. Glass transition temperature, T_g (E'' peak temperature), are listed in Table IV. It can be observed that T_g, moves to higher temperatures till Si69 content is 5 wt %. At the Si69 content of 10 wt %, the T_g is smaller than that at the Si69 content of 10 wt %. The E'' peak values exhibit a decreased trend with Si69 adding to 5 wt % and then increase. Since more and more rubber chains participate in the bound rubber layer at the vicinity of filler surface and the fixed rubber chains do not contribute to molecular slippage,[31] the declining trend of E'' peak values is observed. The increased T_g at the Si69 content of 10 wt % can be explained by the fact that the motion of rubber molecular chains is restricted due to strong filler–rubber interaction and more energy is used for relaxation, so relaxation peak moves to higher temperature.

Real-Time Photographing

Figures 7 and 8 present real-time observations of the crack tip morphologies of silica-filled NR with different Si69 contents at $T = 1200$ and 800 J/m^2. As it is observed in Figure 7, tensile loading direction is indicated by white arrows and the propagation direction is normal to the photomicrograph. The crack tip is composed of a number of dimple zones separated by ligaments. The pattern of ligaments and dimple zones can be described as multiscaled because the large dimple zones delimited by large ligaments are themselves made up of smaller zones delimited by smaller ligaments.[32,33] Compared with other images, ligaments in Figure 7(d) are thinner and more homogeneously distributed on the crack tip. Figure 7(a) and (e) shows the thickest ligaments and the most non-uniform distribution. Figure 7(b) shows both thick and thin ligaments exist. These ligaments are relatively homogeneously distributed. Figure 7(c) shows that the crack tip is consisted of alternating intermediate-sized and thin ligaments. Figure 8 presents that the crack tip morphologies observed at 800 J/m^2 show the same characters.

It has been mentioned in the present studies that the crack propagation is concerned with cracking surface energy dissipation. Two factors can affect the surface energy dissipation at the crack tip. The first factor is associated with the energy necessary to break the bonds at crack tip, and the second factor is attributed to the cracking surface area.[29,30] Silica particles in the matrix build-up a strong filler network and show low interactions with the polymer. But once the Si69 is used, the chemical bonds between the silica surface and the polymer are formed. As we can see in the SEM image in Figure 9, the dispersion of silica in NR matrix become more and more homogeneous until the Si69 content reaches 5 wt %. Thereafter, some silica particles are agglomerated (10 wt % Si69). So, the addition of Si69

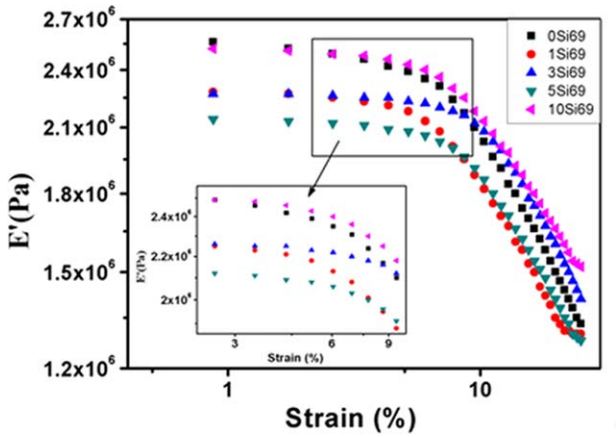

Figure 5. Plots of storage modulus versus strain for silica-filled NR with different contents of Si69. [Color figure can be viewed in the online issue, which is available at wileyonlinelibrary.com.]

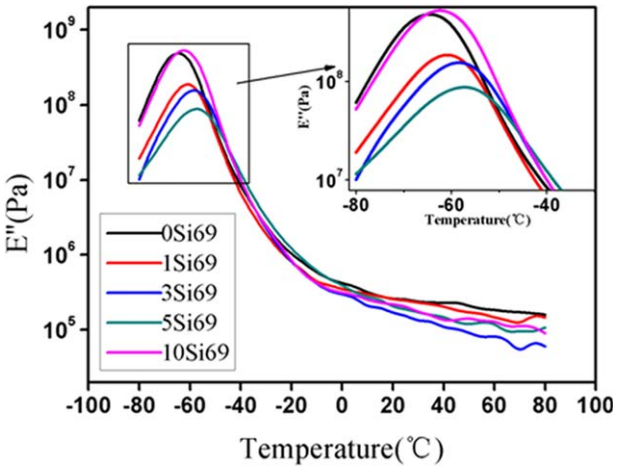

Figure 6. Loss modulus curves of composites as a function of temperature. [Color figure can be viewed in the online issue, which is available at wileyonlinelibrary.com.]

Table IV. Detailed Information of Viscoelasticity of NR/Silica/Si69

Composite	T_g (°C)	E''_{max} (MPa)
0Si69	−65	529
1Si69	−60	207
3Si69	−53	165
5Si69	−55	91
10Si69	−62	546

creates more strong chemical bonds as the Si69 content increases from 0 to 5 wt %. The newly formed bonds increase the energy necessary to break the chemical bonds at the crack tip, hinder the slippages between the matrix chains and silica particles. Therefore, the crack resistance is improved according to the first factor proposed above. Since the Si69 content of 10 wt % is too high, excessive Si69 may lead to excessive crosslinking between silica particles. Thus, silica particles aggregate at Si69 content of 10 wt %. Moreover, the crack tip morphology investigation suggests that ligaments become thinner and more homogeneously distributed with the increase of Si69 content. The thinner ligaments with homogeneous distribution on the crack tip effectively increase the cracking surface area, which implies that higher energy is needed for cracking. Considering these two reasons, we propose that the addition of Si69 can improve the crack resistance of silica-filled NR.

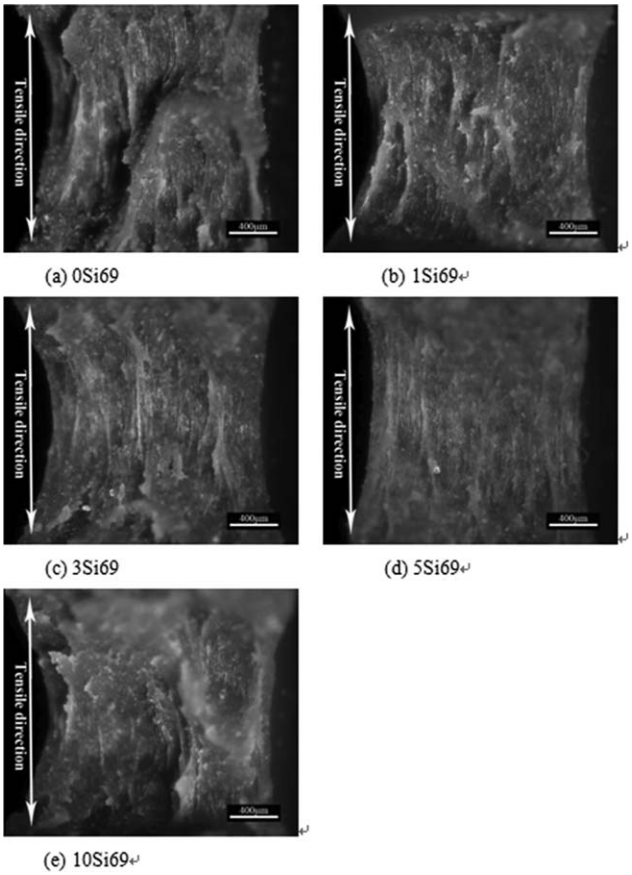

Figure 7. Real-time observation of silica-filled NR with different Si69 contents at tearing energy of 1200 J/m^2.

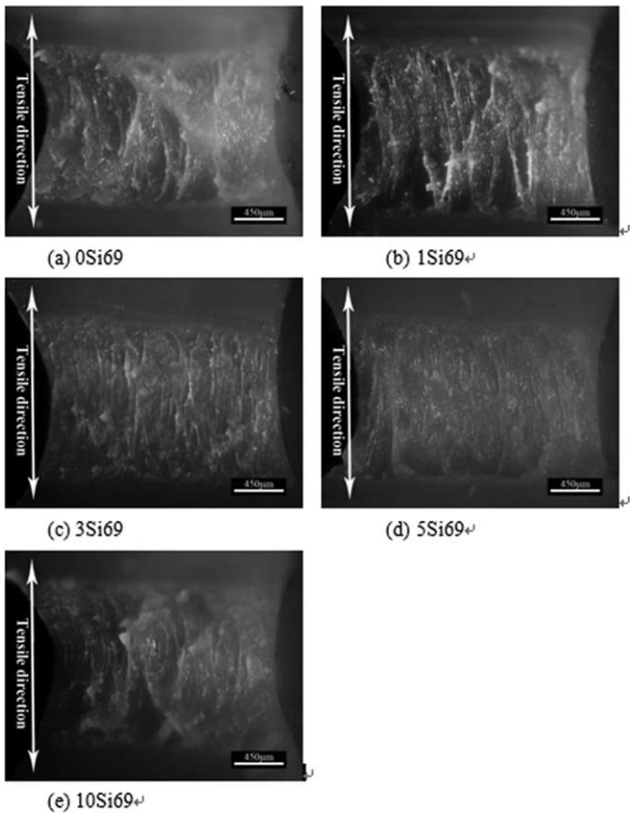

Figure 8. Real-time observation of silica-filled NR with different Si69 contents at tearing energy of 800 J/m^2.

CONCLUSIONS

The influence of Si69 content on the viscoelastic and crack-growth behavior of silica-filled NR was carefully analyzed. The studies on the viscoelastic properties show that the interaction between filler and rubber can be improved obviously when 3 and 5 wt % Si69 are applied. The crack-growth rate is remarkably decreased with the content of Si69 gradually increasing to 5 wt %. It is considered that the decrease of crack-growth rate at the Si69 content of 3 and 5 wt % is due to the increased magnitude of filler–rubber interaction and the good dispersion of silica. The real-time observation and SEM analysis prove that

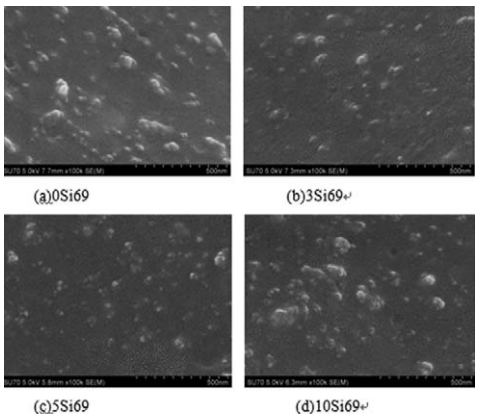

Figure 9. SEM images of NR/Silica/Si69 with 0, 3, 5, 10 wt % Si69 content.

appropriate content of Si69 can make silica homogeneously dispersed in NR matrix, which increases the energy necessary to break the chemical bonds at the crack tip. The thin ligaments with homogeneous distribution on the crack tip effectively increase the surface energy of cracking, which also leads to the decrease of crack-growth rate.

ACKNOWLEDGMENTS

The authors warmly thank the financial support of National Natural Science Foundation of China (Grant No. 21404063), Zhejiang Provincial Natural Science Foundation of China (Grant No. LQ14E030001). The authors are also grateful for the financial support of Ningbo Key Laboratory of Specialty Polymers (Grant No. 2014A22001) and K.C. Wong Magna Fund of Ningbo University.

REFERENCES

1. Stockelhuber, K.; Svistkov, A.; Pelevin, A.; Heinrich, G. *Macromolecules* **2011**, *44*, 4366.
2. Mathew, G.; Huh, M. Y.; Rhee, J.; Lee, M. H.; Nah, C. *Polym. Adv. Technol.* **2004**, *15*, 400.
3. Ou, Y. C.; Yu, Z. Z.; Vidal, A.; Donnet, J. *J. Appl. Polym. Sci.* **1996**, *59*, 1321.
4. Ou, Y.-C.; Yu, Z.-Z.; Vidal, A.; Donnet, J. *Rubber Chem. Technol.* **1994**, *67*, 834.
5. Suzuki, N.; Ito, M.; Yatsuyanagi, F. *Polymer* **2005**, *46*, 193.
6. Heinrich, G.; Vilgis, T. *KGK. Kautschuk Gummi Kunststoffe* **2008**, *61*, 370.
7. Arrighi, V.; McEwen, I.; Qian, H.; Serrano Prieto, M. *Polymer* **2003**, *44*, 6259.
8. Berriot, J.; Lequeux, F.; Monnerie, L.; Montes, H.; Long, D.; Sotta, P. *J. Non-Cryst. Solids* **2002**, *307*, 719.
9. Berriot, J.; Montes, H.; Lequeux, F.; Long, D.; Sotta, P. *Macromolecules* **2002**, *35*, 9756.
10. Mele, P.; Da Silva, C.; Marceau, S.; Brown, D.; De Puydt, Y.; Alberola, N. D. *Macromol. Symp.* **2003**, 185.
11. Mélé, P.; Marceau, S.; Brown, D.; de Puydt, Y.; Albérola, N. D. *Polymer* **2002**, *43*, 5577.
12. Morozov, I.; Svistkov, A.; Heinrich, G.; Lauke, B. *Polym. Sci. Ser. A* **2007**, *49*, 292.
13. Persson, B.; Albohr, O.; Heinrich, G.; Ueba, H. *J. Phys.: Condens. Matter* **2005**, *17*, R1071.
14. Ganesan, L.; Bhattacharyya, P.; Bhowmick, A. K. *Rubber Chem. Technol.* **1995**, *68*, 132.
15. Hamed, G.; Huang, M. *Rubber Chem. Technol.* **1998**, *71*, 846.
16. Rivlin, R.; Thomas, A. G. *J. Polym. Sci.* **1953**, *10*, 291.
17. Tijssens, M.; Van der Giessen, E. *Polymer* **2002**, *43*, 831.
18. Cho, K.; Jang, W. J.; Lee, D.; Chun, H.; Chang, Y.-W. *Polymer* **2000**, *41*, 179.
19. Kim, J.-H.; Jeong, H.-Y. *Int. J. Fatigue* **2005**, *27*, 263.
20. Le Cam, J.-B.; Huneau, B.; Verron, E.; Gornet, L. *Macromolecules* **2004**, *37*, 5011.
21. Flory, P. J. Principles of Polymer Chemistry; Cornell University Press: New York, **1953**.
22. Bala, P.; Samantaray, B.; Srivastava, S.; Nando, G. *J. Appl. Polym. Sci.* **2004**, *92*, 3583.
23. Ansarifar, A.; Lim, H.; Nijhawan, R. *Int. J. Adhes. Adhes.* **2004**, *24*, 9.
24. Lake, G.; Lindley, P. *J. Appl. Polym. Sci.* **1965**, *9*, 1233.
25. Mars, W.; Fatemi, A. *Int. J. Fatigue* **2002**, *24*, 949.
26. Lake, G. *Rubber Chem. Technol.* **1995**, *68*, 435.
27. Nie, Y.; Wang, B.; Huang, G.; Qu, L.; Zhang, P.; Weng, G.; Wu, J. *J. Appl. Polym. Sci.* **2010**, *117*, 3441.
28. Weng, G.; Yao, H.; Chang, A.; Fu, K.; Liu, Y.; Chen, Z. *RSC Adv.* **2014**, *4*, 43942.
29. Fröhlich, J.; Niedermeier, W.; Luginsland, H.-D. *Compos. Part A: Appl. Sci. Manuf.* **2005**, *36*, 449.
30. Luginsland, H.-D.; Frohlich, J.; Wehmeier, A. *Rubber Chem. Technol.* **2002**, *75*, 563.
31. Qu, L.; Yu, G.; Xie, X.; Wang, L.; Li, J.; Zhao, Q. *Polym. Compos.* **2013**, *34*, 1575.
32. Beurrot, S.; Huneau, B.; Verron, E. *J. Appl. Polym. Sci.* **2010**, *117*, 1260.
33. Weng, G.; Huang, G.; Lei, H.; Qu, L.; Nie, Y.; Wu, J. *Polym. Degrad. Stab.* **2011**, *96*, 2221.